LUNAR BASALTIC VOLCANIC ERUPTIONS: GAS RELEASE PATTERNS AND VARIATIONS IN LAVA VESICULARITY: 1. LAVA PONDS, SHIELD VOLCANOES, FOAMS, AND IRREGULAR MARE PATCH (IMP) MORPHOLOGY. L. Wilson[1] and J. W. Head[2], [1]Lancaster Environment Centre, Lancaster University, Lancaster LA1 4YQ, UK, l.wilson@lancaster.ac.uk, [2]Department of Earth, Environmental and Planetary Sciences, Brown University, Providence, RI 02912 USA, james_head@brown.edu.

Introduction: We outline the basic principles of lunar volcanism and show how localized vents control the formation of lava ponds, small shield volcanoes, foams, and irregular mare patches (IMPs). In a companion abstract [1] we deal with much more elongate fissure vents and show how these lead to mare sheet flows and ring-moat dome structures (RMDSs).

Influence of dike origin and emplacement: The nature of the eruptive activity at various stages in lunar eruptions was dictated by the origin of the dikes feeding the eruptions. Lack of crustal contamination points to most lunar basaltic eruptions being fed by dikes that nucleated in deep mantle source zones, grew upward slowly (decades?) until their vertical extents were tens of km, and then abruptly disconnected from their sources to migrate upward very quickly (hours) through the mantle and crust [2]. This great vertical dike extent meant that the major lunar magmatic volatile, CO, was produced in amounts up to 2000 ppm by mass over a wide range of depths in the dike, potentially extending down to at least 50 km. Up to at least 1000 ppm of water and sulphur compounds was released in the upper few hundred meters of dikes [3].

Characteristics of lunar volcanism: Basaltic volcanic eruptions on the Moon took place in conditions of low acceleration due to gravity and negligible atmospheric pressure, causing essentially all lunar eruptions to have an explosive component. However, the lunar versions of hawaiian and strombolian explosive activity differed greatly from those on Earth [4], with no lunar analog of a convecting plinian eruption cloud [2]. The extreme expansion of even the smallest gas bubbles produced pyroclasts predominantly of sub-mm size. As a result, lunar fire fountains produced in eruptions with high mass fluxes and low volatile contents (a few hundred ppm) were optically dense [4]. Most pyroclasts within such fountains were unable to radiate heat into space and thus landed at magmatic temperature to coalesce into lava that, having lost almost all of its gas, was neary completely vesicle-free.

Pyroclasts were always dispersed ballistically after an acceleration phase as magmatic gas expanded away from the vent into the vacuum. Some lunar magmas were relatively volatile rich and produced fountains that were less optically dense. Total magma volatile mass fractions up to 2000 ppm [3] led to pyroclast speeds in steady eruptions of up to 180 m/s and maximum ranges of ~20 km. Greater speeds and ranges were possible in the initial stages of eruptions as gas concentrated in the upper tips of dikes was released, producing regional pyroclastic blankets [2].

Since all eruptions began with the arrival of a dike at the surface, initial vents were always fissures. If the fissure length was much less than the maximum range of the pyroclasts, gas effectively expanded radially from a point source, producing a circular, umbrella-shaped fire fountain like those seen on Io [5], though of very much smaller size [6] due to the much smaller volatile contents of the lunar magmas [7]. If the fissure length was greater than the maximum pyroclast range, gas would mainly have expanded sideways away from the fissure, not radially. These differing patterns of gas expansion and clast dispersal cause a concentration of clasts in the outer edges of elongate fountains, enhancing their optically density.

Evolution of an eruption: Volatile concentration into the low-pressure region near the upper tip of the propagating dike causes the transient opening Phase 1 of the eruption to be very explosive [8]. Phase 2, during which the dike as a whole is still rising toward a neutral buoyancy configuration, generally has the highest magma discharge rate, and involves the near-steady explosive eruption of magma with a volatile content representative of the bulk of the magma. Efficient gas loss from the fire fountain causes lava flowing away from the vent to be largely vesicle-free.

Phase 3 begins when the dike feeding the eruption reaches an equilibrium, with the positive buoyancy of its lower part in the mantle balancing the negative buoyancy of its upper part in the crust. The lower dike tip then stops rising and the dike's vertical extent becomes fixed. The process driving this phase of the eruption becomes the horizontal reduction in the thickness of the dike as both its internal excess pressure, and the forced deformation of the host rocks by the intrusion of the dike, relax [2]. While deformation of host rocks in the shallow crust is probably elastic and rapid, deformation of hot mantle rocks surrounding the lower part of the dike is visco-elastic or viscous, resulting in a much longer time scale. During this period, the vertical rise speed of the magma decreases greatly, implying that the magma volume flux leaving the vent similarly decreases. The reduced vertical magma flow speed means that gas bubbles, previously nucleating throughout the vertical extent of the dike, can now rise through the liquid. With a stable vertical pressure dis-

tribution in the dike, no more gas is released anywhere in the dike and CO bubbles formed at great depth together with H_2O and sulfur compounds released at shallow depths can migrate upward to continue to drive hawaiian explosive activity at the vent for a while, with a change to strombolian activity as extensive bubble coalescence occurs.

Phase 4 begins when all of the deep-sourced gas has migrated out of the surface vent. Explosive activity becomes minimal or stops and a stable crust forms on the magma still emerging from the vent and flowing away as lava. The duration of this final phase of the eruption would have been influenced significantly by the nature and magnitude of the global stress state of the lithosphere. Lunar thermal history [9] suggests the presence of extensional stresses in the lithosphere for the first ~1-1.5 Ga as radiogenic heat accumulated and fed the onset of mare volcanism, followed by compressive stresses over the last ~3 Ga as the interior cooled. Compression encourages efficient dike closure, implying that more of the magma originally contained by the dike would have erupted during the explosion-free, vesicle-rich effusion phase 4 of the most recent eruptions in a given lunar volcanic province.

The consequences of these various phases of activity would have depended critically on the vent configuration and the magma discharge rate [6] during the various stages of the eruption. We identify four different environments as follows: 1. Summit pit craters on shield volcanoess (e.g., Ina); 2. Calderas associated with intersecting dikes (e.g., Hyginus); 3. Linear depressions above dikes (e.g., Sosigenes); and 4. Topographically uncontained linear vents above fissure eruptions in the maria (e.g., most mare IMPs). We now address the first two of these environments.

Summit pits on shield volcanoes: Shield volcanoes form on the Moon in eruptions where both the volume flux erupted from the vent and the magma volatile content are relatively small. They also appear to commonly involve only short fissure vents, so that although the low volatile content causes short pyroclast ranges, nevertheless a small and roughly circular lava pond forms around the vent. Overflows from the pond are fed at the low eruption volume flux and resulting lava flows do not travel far before stopping due to cooling. Previous flow deposits form obstacles to lava overflowing the pond and so eventually flows will have left the pond in all radial directions and a low shield volcano progressively accumulates [6]. As long as explosive activity continues in the vent (phases 1-3) the lavas forming the bulk of the shield are volatile-depleted and vesicle-free. With an undisrupted and cooling crust on the pond in phase 4, however, magma being squeezed out of the closing dike exsolves ~1000 ppm of water and sulphur componds over the last few hundred meters of its rise and the resulting extremely vesicular lava foam intrudes under the pond crust, causing vertical stresses and eventually fractures [10]. Foam erupts onto the surface of the pond forming characteristic low mounds which represent one type of irregular mare patch (IMP) [11]. Examples include Ina [12] (Fig. 1) and Cauchy-5 [13]. The foam consists of very small (10-20 μm) gas bubbles, stabilized against exploding into the overlying vaccum by surface tension forces [9], soon aided by radiative cooling.

Calderas: The most complex case of a lunar volcanic depression is represented by Hyginus. The depression marks the intersection of at least 2 dikes and has been modeled as a collapse caldera [14] as its feeding dikes lost volatiles through smaller collapse craters above the dikes. The presence of numerous IMPs [11] implies that late-stage (phase 4) extrusion of foam onto the floor of the caldera took place.

Additional results: The remaining vent and eruption environments listed earlier [3. Linear depressions above dikes (e.g., Sosigenes [15]); and 4. Topographically uncontained linear vents above fissure eruptions in the maria (e.g., most mare IMPs)] are explored in detail in a companion abstract [1].

References: [1] Wilson L. & Head J. W. (2018) This meeting. [2] Wilson L. & Head J. W. (2017) *Icarus, 283*, 146-175. [3] Rutherford M. J. et al. (2017) *Amer. Mineralogist, 102,* 2045-2053. [4] Wilson L. & Head J. W. (1981) *JGR, 86*, 2971-3001. [5] Wilson L. & Head J. W. (2001) *JGR, 106*, 32,997-33,004. [6] Head J. W. et al. (2002) JGR, 107, 5001, 17 pp. [7] Head J. W. & Wilson L. (2017) *Icarus, 283*, 176-223. [8] Wilson L. & Head J. W. (2003) *GRL, 30*, 1605, 4 pp. [9] Solomon S. C. & Head J. W. (1980) *Rev. Geophys. Space Phys., 18*, 107-141. [10] Wilson L. & Head J. W. (2017) *JVGR, 335*, 113-127. [11]. Braden S. E. et al. (2014) *Nature Geosci., 7*, 787-791. [12] Qiao L. et al. (2017) *Geology, 45*, 455-458. [13] Qiao L. et al. (2018) This meeting. [14] Wilson L. et al. (2011) *Icarus, 215*, 584-595. [15] Qiao L. et al. (2017) *MAPS*, doi:10.1111/maps.13003

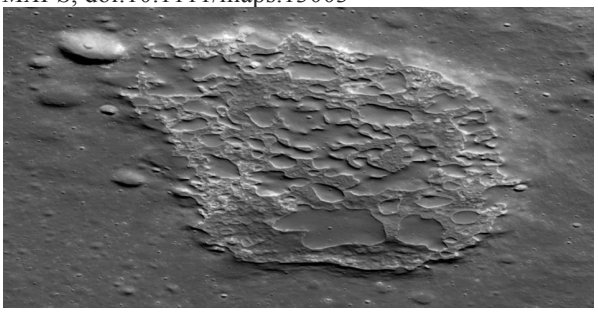

Figure 1 Oblique view of the Ina IMP. NASA Lunar Reconnassance Orbiter Camera image.